



Conductive zigzag Pd(III)–Br chain complex realized by multiple-hydrogen-bond approach

Journal:	<i>CrystEngComm</i>
Manuscript ID	CE-ART-03-2020-000332.R1
Article Type:	Paper
Date Submitted by the Author:	24-Apr-2020
Complete List of Authors:	Mian, Mohammad; Tohoku University, Department of Chemistry, Graduate School of Science Afrin, Unjila; Tohoku University, Chemistry Iguchi, Hiroaki; Tohoku University, Department of Chemistry, Graduate School of Science Takaishi, Shinya; Tohoku University, Chemistry Yoshida, Takefumi; Tohoku University, WPI-Advanced Institute for Materials Research Miyamoto, Tatsuya; The university of Tokyo, Applied Physics Okamoto, Hiroshi; The university of Tokyo, Applied Physics Tanaka, Hisaaki; Nagoya University, Department of Applied Physics Kuroda, Shin-ichi; Nagoya University, Department of Applied Physics Yamashita, Masahiro; Tohoku University, Chemistry

ARTICLE

Conductive zigzag Pd(III)–Br chain complex realized by multiple-hydrogen-bond approach

Received 00th January 20xx,
Accepted 00th January 20xx

DOI: 10.1039/x0xx00000x

Mohammad Rasel Mian,^{†a,b} Unjila Afrin,^{†a} Hiroaki Iguchi,^{*a} Shinya Takaishi,^a Takefumi Yoshida,^b Tatsuya Miyamoto,^c Hiroshi Okamoto,^{c,d} Hisaaki Tanaka,^e Shin-ichi Kuroda^e and Masahiro Yamashita^{*a,b,f}

Coexistence of zigzag structure and uncommon Pd(III) oxidation state in quasi-1D halogen-bridged metal complexes was realized in a conductive Br-bridged Pd chain complex, [Pd(dabdOH)₂Br]SO₄·3H₂O (**2**), for the first time. Intra- and interchain hydrogen-bond network among (2S,3S)-2,3-diaminobutane-1,4-diol (dabdOH) ligand, SO₄²⁻ and H₂O molecules support this unusual structure and the electronic state. The electrical conductivity of **2** reached 0.05 S cm⁻¹ at room temperature.

Introduction

The chemistry of Pd(III) oxidation state has garnered much attention from researchers in the field of catalysis.¹⁻⁴ The Pd(III) states are however still rare even nowadays, particularly in materials with good crystallinity. Recently, researchers have been attracted a lot of interests in Pd(III) compounds from the viewpoint of their solid state functionalities. For example, the one-dimensional (1D) array of Pd(III) ions, which have unpaired electron in each d_z^2 orbital, are expected to show semiconducting behavior⁵ and other phenomena based on strongly correlated electron system.⁶ However, there is few 1D Pd(III) compounds with Pd–Pd bonds that allow for the rational control of electrical conductivity because of their air and thermal instability.⁵

From this point of view, quasi-1D halogen-bridged metal complexes (MX chains) are promising alternatives for enhancing the functionality of 1D Pd(III) compounds. Although many 1D Br-bridged Pd complexes (hereafter abbreviated as PdBr chains) have been reported, the vast majority of them fall into Pd(II/IV) mixed valence (MV) state (…Pd^{II}…Br–Pd^{IV}–Br…Pd^{II}…Br–Pd^{IV}–Br…).⁷ The Pd(III) averaged valence (AV) state (–Pd^{III}–Br–Pd^{III}–Br–) is quite rare and is achieved only if

the Pd…Pd distance along the chain ($d(\text{Pd}\cdots\text{Pd})$) is shorter than 5.26 Å.⁸ Some approaches successfully shortened the ($d(\text{Pd}\cdots\text{Pd})$) and achieved Pd(III) AV state. For instance, introducing counteranions with long alkyl chains decreased $d(\text{Pd}\cdots\text{Pd})$ by the attractive force among alkyl moieties. Single-crystalline PdBr chains, [Pd(en)₂Br](Y)₂·H₂O (en = ethylenediamine, Y = dipentylsulfosuccinate (**C5S**), diheptylsulfomalonate (**C7M**)), exhibited a MV-AV transition at 206 K for **C5S**⁹ and at 310 K for **C7M**.¹⁰ Changing in-plane ligands to 1*R*,2*R*-diaminocyclopentane (cptn) also affected the electronic state. [Pd(cptn)₂Br]Br₂ showed the MV/AV phase separation phenomenon between 130 to 50 K.¹¹ Consequently, it has been difficult to realize the Pd(III) AV state above room temperature (RT).

A new strategy so-called *multiple-hydrogen-bond approach* was recently reported in a PdBr chain, [Pd(dabdOH)₂Br]Br₂ (**1**) (dabdOH = (2S,3S)-2,3-diaminobutane-1,4-diol).¹² The additional hydrogen bonds originating from hydroxy groups of dabdOH increased the interchain distance, resulting in the shortest $d(\text{Pd}\cdots\text{Pd})$ (5.182 Å at 93 K) of all PdBr chains reported so far. Moreover, the new approach stabilized the Pd(III) AV state in **1** up to the decomposition temperature (443 K). The short $d(\text{Pd}\cdots\text{Pd})$ enhanced the orbital overlap between $4d_z^2$ (Pd) and $4p_z$ (Br) orbitals, yielding the good conductive performance (3–38 S cm⁻¹ at RT) comparable to other highly conductive coordination polymers.¹³ This approach was also effective to shorten $d(\text{Pt}\cdots\text{Pt})$ in the PtX-chain analogues, [Pt(dabdOH)₂X]X₂ (X = Cl, Br).¹⁴

Although the *multiple-hydrogen-bond approach* was useful in PdBr and PtX chains containing halide counteranions as discussed above, its applicability to other counteranion system has been unclear. In this work, we introduced SO₄²⁻ as the counteranion which acts as anisotropic hydrogen-bond acceptor. The synthesis and structural characterization of [Pd(dabdOH)₂Br]SO₄·3H₂O (**2**) are presented, together with its optical and electrical properties.

^a Department of Chemistry, Graduate School of Science, Tohoku University, 6-3 Aza-Aoba, Aramaki, Sendai 980-8578, Japan.

^b Advanced Institute for Materials Research, Tohoku University, 2-1-1 Katahira, Aoba-ku, Sendai 980-8577, Japan

^c Department of Advanced Materials Science, Graduate School of Frontier Sciences, The University of Tokyo, Kashiwa 277-8561, Japan.

^d AIST-UTokyo Advanced Operando-Measurement Technology Open Innovation Laboratory, National Institute of Advanced Industrial Science and Technology, Chiba 277-8568, Japan.

^e Department of Applied Physics, Graduate School of Engineering, Nagoya University, Chikusa, Nagoya 464-8603, Japan.

^f School of Materials Science and Engineering, Nankai University, Tianjin 300350, China

†M. R. M. and U. A. contributed equally.

†Electronic Supplementary Information (ESI) available: Crystallographic data and magnified ESR spectrum. See DOI: 10.1039/x0xx00000x

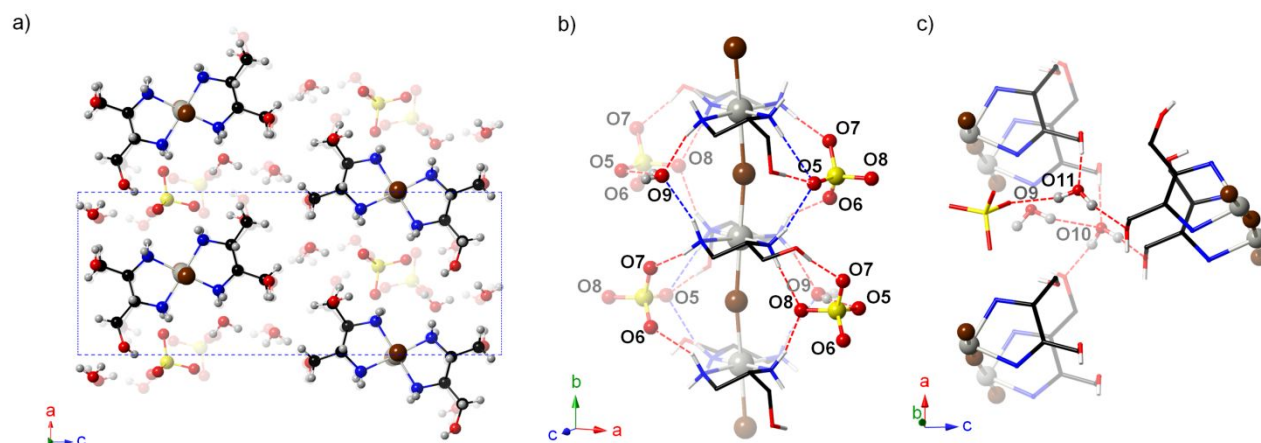


Fig. 1 a) Crystal structure of **2**. b) Zigzag chain structure and intrachain hydrogen-bond network of **2**. H atoms connected to the C atoms and two of four CH₂OH groups unrelated to the intrachain hydrogen-bond network are omitted for clarity. c) Interchain hydrogen-bond network around two H₂O molecules (O10 and O11) in **2**. Half of each chain and H atoms connected to the C and N atoms are omitted for clarity. Hydrogen bonds are shown in dashed lines (red: O...X distance < 3.0 Å, blue: O...X distance > 3.0 Å, X = N or O) in b) and c). Gray, Pd; brown, Br; yellow, S; red, O; blue, N; black, C; Light gray, H.

Results and Discussions

Synthesis and crystal structure

Slow Br₂ vapor diffusion from its 1,4-dioxane solution to the solution of [Pd(dabdOH)₂]Br₂ and Na₂SO₄ at 10 °C gave copper-lustrous rod-like crystals of **2**. X-ray crystallographic analysis revealed that 1D Pd–Br chain structure was formed with SO₄²⁻ counteranions. **2** crystallized in the chiral space group *P*2₁2₁2₁, and the absolute structure was determined by *S,S* configuration of the dabdOH, consistent with the fact that the Flack parameter is closed to zero (0.008(5)). The crystal structure of **2** and its refinement data at 93 K are shown in Fig. 1a and Table 1, respectively. The refinement data from 150 to 300 K are shown in the ESI[†].

The 1D chain structure of **2** is supported by intrachain hydrogen-bond network among amino groups of dabdOH, SO₄²⁻ counteranions and H₂O molecules (containing O9 atom) extending along *b* axis (Fig. 1b). Moreover, the chains are connected each other via interchain hydrogen-bond network. The SO₄²⁻ counteranions connect adjacent chains along *a* axis, and two H₂O molecules (containing O10 and O11 atoms) connect three chains to extend the network along *c* axis (Fig. 1c). The red and blue dashed lines in Fig. 1b,c indicate the hydrogen bonds whose O...X distance (X = N or O) is shorter or longer than 3.0 Å, respectively. Apparently, most of the hydrogen bonds are coloured in red and can be classified into "strong" hydrogen bond.¹⁵ This is in contrast to the CH₃...O "weak" hydrogen bond length (3.48 Å) observed in the PdBr chain with (3*S*,4*S*)-3,4-diaminohexane (hxn) ligands.^{15,16} In addition, two-fold periodicity, which is structural characteristic of MV state, was observed in **2**, whereas it originates mainly from the packing manner of SO₄²⁻ counteranions and H₂O molecules.

Table 1. Crystallographic Data for **2**.

2	
Radiation type, wave length /Å	MoKα, 0.7107
Empirical formula	C ₈ H ₃₀ BrN ₄ O ₁₁ PdS
Formula weight	576.73
Crystal system	orthorhombic
Space group	<i>P</i> 2 ₁ 2 ₁ 2 ₁
Crystal size /mm ³	0.15 × 0.03 × 0.02
<i>a</i> /Å	8.4228(3)
<i>b</i> /Å	10.2975(3)
<i>c</i> /Å	21.9679(6)
<i>V</i> /Å ³	1905.36(10)
Temperature / K	93
<i>Z</i>	4
Density(calculated) / gcm ⁻³	2.010
Absorption coefficient /mm ⁻¹	3.241
<i>R</i> 1, <i>wR</i> 2 [<i>I</i> > 2σ(<i>I</i>)]	0.0255, 0.0508
<i>R</i> 1, <i>wR</i> 2 [all data]	0.0299, 0.0519
<i>F</i> (000)	1164
Goodness of fit on <i>F</i> ²	1.039
Flack parameter	0.008(5)

The *d*(Pd...Pd) of **2** is determined to be 5.1494(2) Å, which breaks a previous shortest record in **1** (5.182 Å). It is however noteworthy that the Pd–Br chain structure of **2** is slightly bent ($\angle(\text{Pd–Br–Pd}) = 171.74^\circ$) and the sum of two Pd–Br bond lengths (*d*(Pd–Br) = 2.5757(5) Å and 2.5872(5) Å) is 5.1629(10) Å. The temperature dependence of *d*(Pd...Pd) (Fig. 2a) shows that the slope of the lines for **1** and **2** are almost comparable but smaller than that for **C55**. This result demonstrates the rigid packing character of **2** as well as **1**, compared with **C55**, which contains soft alkyl moiety. Despite the existence of lattice H₂O molecules, the rigidity of **2** is derived from the "strong" hydrogen-bond networks in the crystal discussed above. The $\angle(\text{Pd–Br–Pd})$ of **2** gradually increased with increasing temperature, though it is far from the straight chain (180°) even at RT (Fig. 2b).

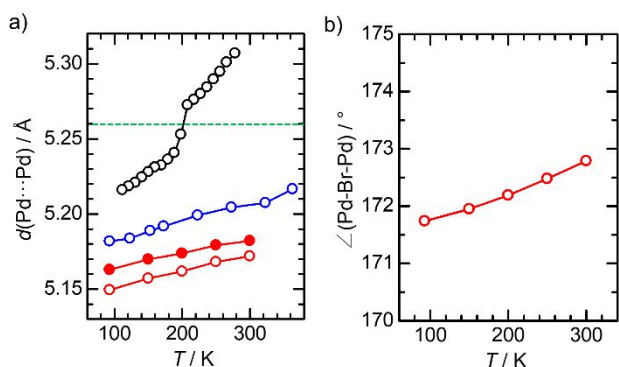


Fig. 2 a) Temperature dependence of $d(\text{Pd}\cdots\text{Pd})$ (open circle) in **2** (red), **1** (blue), **C5S** (black) and the sum of two Pt-Br bond lengths in **2** (filled red circle). Green broken line shows the reported MV-AV border. b) Temperature dependence of $\angle(\text{Pd-Br-Pd})$.

The electronic state of **2** is likely to be the Pd(III) AV state, because $d(\text{Pd}\cdots\text{Pd})$ is quite shorter than the predicted MV-AV border (5.26 Å; green broken line in Fig. 2a) and the bridging Br⁻ is almost equidistant from the two neighbouring Pd ions. Since the zigzag MX-chain structure has been reported only in some complexes with relatively long $d(\text{M}\cdots\text{M})$,¹⁷ **2** is the first one with $d(\text{M}\cdots\text{M})$ shorter than 5.26 Å.

Determination of electronic state

Polarized Raman spectroscopy is the powerful tool for determining the electronic state of MX chains. It has been well known that MX chains in MV state show characteristic Raman signals attributed to X-M^{IV}-X symmetrical stretching mode ($\nu(\text{X-M}^{\text{IV}}-\text{X})$).¹⁶⁻¹⁹ On the other hand, ($\nu(\text{X-M}^{\text{III}}-\text{X})$) is forbidden in the AV state because the bridging Br⁻ ions are at the midpoint between two M atoms.^{9,11,12} In order to confirm the electronic state, we acquired the polarized Raman spectrum of **2** at RT. As it is clearly shown in Fig. 3a, no peaks were observed in **2** as well as reported PdBr chains such as **C5S** (100 K) and **1**, whereas $\nu(\text{Br-Pd-Br})$ is typically observed around 130 cm⁻¹ in the Pd(II/IV) MV state.^{9,11} This result strongly supports that **2** forms the Pd(III) AV state. The X-ray absorption fine structure (XAFS) spectra of **1** and **2** (Fig. 3b) were almost identical, consistent with their similarity in the coordination geometry and electronic state of the Pd ion.²⁰

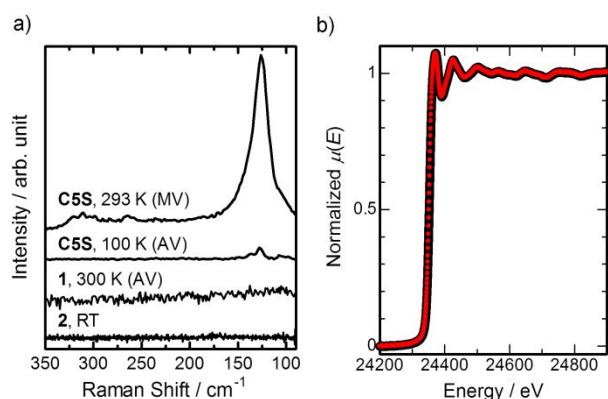


Fig. 3 a) Polarized Raman spectrum of **2** at RT. The spectra of **C5S** at 293 K (MV state), at 100 K (AV state), and **1** at 300 K (AV state) are shown for comparison. All spectra were measured parallel to the chain axis. The excitation wavelength is 632.8 nm. b) X-ray absorption spectra around Pd-K edge of **1** (black line)²⁰ and **2** (red dots) at 50 K.

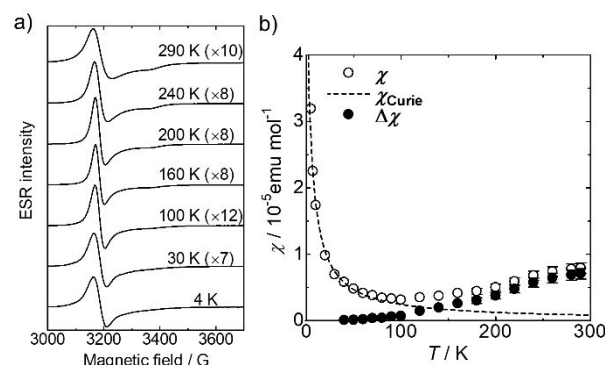


Fig. 4 Temperature dependence of a) ESR spectra and b) spin susceptibility (χ) of **2**. Hollow circles, χ ; Filled circles, $\Delta\chi = \chi - \chi_{\text{Curie}}$; Dashed line, Curie law with 0.06% spin impurities.

For further confirmation, Electron-spin resonance (ESR) spectra of polycrystalline sample of **2** were acquired. Fig. 4a shows temperature dependence of the ESR spectra. The g values were calculated to be $g_{\perp} = 2.1295$ and $g_{\parallel} = 2.0119$ from the spectrum at 240 K (Fig. S1, ESI[†]), supporting that the spin exists in d_{z^2} orbital of Pd ion. These g values are similar to those in **1** ($g_{\perp} = 2.1248$ and $g_{\parallel} = 2.0016$), thus the electronic state of **2** is close to that of **1**, despite the bent chain structure. The temperature dependence of the molar spin susceptibility (χ) obtained from ESR spectra of **2** is shown in Fig. 4b. The clear Curie-like behaviour derived from 0.06% of the magnetic impurities was observed below 80 K, suggesting that an odd number of Pd(III) ions exist in the domains. $\Delta\chi$, which is defined as the subtraction of the Curie component from χ , gradually decreased with decreasing temperature. This is likely due to a spin-Peierls transition, which was also observed for **1**¹² and **C7M** in a Pd(III) AV state.¹⁰ Because the origin of the spins are Pd(III) species in the whole temperature range, the g values was almost independent from the temperature. The slight broadening of the signal at 290 K is likely due to the enhancement of the spin-lattice relaxation by temperature increase. On the basis of the Raman, XAFS and magnetic studies, it can be concluded that **2** is the first MX chain exhibiting both AV state and zigzag structure.

Thermal stability

Thermogravimetric analysis (TGA) and differential thermal analysis (DTA) were performed on **2** in order to study its thermal stability. As shown in TGA trace (Fig. 5), the initial 6.8% weight loss was observed from 320 K to 365 K, followed by the second 3.7% weight loss from 365 to 400 K. Both weight loss processes were endothermic as confirmed by the DTA trace. These results agree with the liberation of two H₂O (6.2%) followed by one H₂O (3.1%) from **2**, reflecting the two different environments of H₂O molecules. As discussed above, two H₂O molecules (O10 and O11) contribute to the interchain hydrogen-bond network, and one H₂O molecule (O9) contributes to the intrachain hydrogen-bond network ($\cdots\text{H-N-H}\cdots\text{O}(\text{H}_2)\cdots\text{H-N-H}\cdots$) along the chain axis. It is likely that the latter *intrachain* H₂O molecule is well shielded and resistant to the liberation, compared with the former *interchain* H₂O molecules.

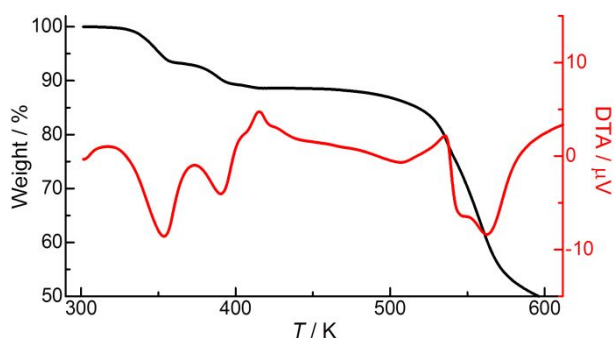


Fig. 5 TGA (black) and DTA (red) trace of **2**.

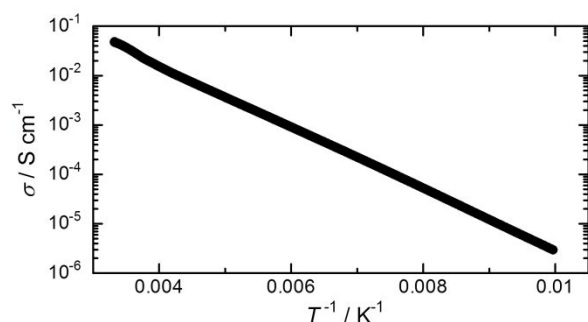


Fig. 6 Temperature dependence of the electrical conductivity (σ) of **2** measured along the chain axis.

Conducting behaviour

The temperature dependence of electrical conductivity (σ) of **2** along the chain direction was measured by four-contact probe method. To check the reproducibility, the measurements were performed in several different single crystals. The σ at RT (σ_{RT}) was in the range of 0.005 to 0.05 S cm⁻¹. In the most conducting crystal, the temperature dependence of σ (Fig. 6) revealed the thermally activated transport in **2**. Fitting the data in the range of 100–300 K with the Arrhenius equation $\sigma = \sigma_0 \exp(E_a/kT)$, where σ_0 is a prefactor, E_a is an activation energy, k is the Boltzmann constant and T is the temperature, gives $E_a \approx 123$ meV, which is larger than that of **1** (96 meV). The σ_{RT} of **2** is two to three orders of magnitude lower than that of **1** in spite of the short $d(\text{Pd}\cdots\text{Pd})$. This is probably because the electron conduction is perturbed due to the zigzag chain structure in **2**. The σ_{RT} is however still higher than previously reported Pd(III)Br chains with long alkyl chains (10^{-8} S cm⁻¹ for **C5S** and 10^{-5} S cm⁻¹ for **C7M**).^{9,10}

Origin of the uncommon structure and electronic state

Herein, we discuss the origin of the short $d(\text{Pd}\cdots\text{Pd})$ and zigzag chain fashion of **2**. As shown in Fig. 1b, each of the three O atoms (O5, O8 and O9) directly connects two amino groups as the monoatomic hydrogen acceptor. Although it is similar to the manner in **1** ($\cdots\text{H}-\text{N}-\text{H}\cdots\text{Br}\cdots\text{H}-\text{N}-\text{H}\cdots$), the small O atoms in **2** can provide the short N \cdots O distance (2.85–3.26 Å) compared with the N \cdots Br distance (3.46–3.53 Å) in **1**,¹²

inducing the short $d(\text{Pd}\cdots\text{Pd})$. Moreover, N \cdots O distance in the side of O8 and O9 atoms (2.85–3.05 Å) is shorter than that in the opposite side with O5 atom (3.10–3.26 Å). In addition, triatomic hydrogen acceptor (O7–S–O6) is also located at the side of O5 atom. This asymmetric and distorted hydrogen-bond system is probably derived from the small van der Waals radius of O atom as the monoatomic hydrogen acceptor, resulting in the zigzag fashion in **2**. The hydroxy groups in dabdOH ligand provide additional hydrogen bonds with SO₄²⁻ and H₂O molecules. The O \cdots O distances between dabdOH and SO₄²⁻ are 2.65 and 2.87 Å. These "strong" hydrogen bonds should reinforce the zigzag chain structure.¹¹

Conclusions

In this work, [Pd(dabdOH)₂Br]SO₄·3H₂O (**2**), which exhibits zigzag structure and the shortest $d(\text{Pd}\cdots\text{Pd})$ of all PdBr chains, was studied. Single crystal structural analysis and spectroscopic studies revealed that **2** is in uncommon Pd(III) oxidation state. The zigzag chain structure is supported by intra- and inter-chain hydrogen-bond network among ligands, SO₄²⁻ and H₂O molecules. **2** displays semiconducting behaviour with high conductivity of 0.005–0.05 S cm⁻¹ at RT despite its zigzag fashion, which is disadvantage for the electron conduction. It is noteworthy that **2** is the first zigzag MX chain in averaged valence (AV) state. This work suggests that *multiple-hydrogen-bond approach* to decrease $d(\text{M}\cdots\text{M})$ is also applicable to MX chains with counteranions other than halide. Since various supramolecular architectures have been reported in PtX-chain analogues,²¹ the *multiple-hydrogen-bond approach* is promising for realizing supramolecular Pd(III)Br chains, which can attract the interest of both chemists and physicists.

Experimental

Synthetic procedures

PdBr₂, Na₂SO₄, MeOH, 1,4-dioxane and Br₂ were obtained by Wako Pure Chemical Industries, Ltd. and used as received. The in-plane ligand dabdOH was synthesized from L-(+)-tartaric acid following a previously reported procedure.^{12,22} Pt(II) complex, [Pd(dabdOH)₂]Br₂, was also synthesized according to the previous report.¹²

Synthesis of [Pd(dabdOH)₂Br]SO₄·3H₂O (2**).** 4 mg (28.2 μmol) of sodium sulfate (Na₂SO₄) and 6 mg (11.8 μmol) of [Pd(dabdOH)₂]Br₂ were dissolved into 0.6 mL of H₂O/CH₃OH (1:2) solution. Single crystal of **2** was obtained by slowly diffusing Br₂ vapor from Br₂/1,4-dioxane solution into the complex solution at 10 °C. Copper-luster rod-like single crystals were obtained a day later. Elemental analysis, Found: C, 16.9; H, 5.3; N, 9.8. Calc. for C₈H₃₀BrN₄O₁₁PdS: C, 16.7; H, 5.2; N, 9.7%.

Methods

Single-crystal X-ray structural determination: Single-crystal X-ray diffraction data were collected on a Rigaku XtaLAB AFC10 diffractometer with HyPix-6000HE hybrid pixel array detector, graphite monochromated Mo K α radiation ($\lambda = 0.7107 \text{ \AA}$) and cryogenic equipment GN-2D/S. The crystal structure was solved by using direct methods (Sir2019),²³ followed by Fourier syntheses. Structure refinement was performed by using full matrix least-squares procedures using SHELXL^{24,25} on F^2 in the Yadokari-XG2009 software.²⁶ CCDC-1987451, 1998640, 1998641, 1998642 and 1998643 contain the supplementary crystallographic data for **2** at 93 K, 150 K, 200 K, 250 K and 300 K, respectively.

Raman spectroscopy: Polarized Raman spectrum was acquired on HORIBA LabRAM HR-800 with He–Ne laser (632.8 nm) and an optical microscope.

X-ray absorption fine structure (XAFS) measurement: XAFS spectra of Pd K-edge were recorded at 50 K by using the NW10A stations at the Photon Factory Advanced Ring (PF-AR) in High Energy Accelerator Research Organization (KEK). Data analyses were performed on the Demeter software platform.²⁷

ESR spectroscopy: ESR spectroscopy were performed on a Bruker EMX spectrometer equipped with a gas-flow type cryostat Oxford ESR 900. The absolute magnitude of the spin susceptibility was calibrated using CuSO₄·5H₂O as a standard.

Thermogravimetric analysis: TGA and DTA were performed by using Shimadzu DTG-60H under N₂ gas flow (50 mL/min) condition with a sweep rate of 5 K/min.

Electrical conductivity measurement: The temperature dependence of the electrical conductivity was measured in a liquid He cryostat of a Quantum Design PPMS (Physical Property Measuring System) model 6000 by using the four-probe method with a cooling rate of 1 K/min. The electrical leads (15 $\mu\text{m}\phi$ gold wires) were attached to a single crystal with carbon paste (Dotite XC-12 in diethyl succinate).

Elemental analysis: Elemental analysis was performed by using J-Science Lab Co. Ltd. JM11 at the Research and Analytical Center for Giant Molecules, Graduate School of Science, Tohoku University.

Conflicts of interest

The authors declare no competing financial interests.

Acknowledgements

This work was partly supported by JSPS KAKENHI Grant Numbers JP15K17828 (H.I.), JP18K14233 (H.I.), JP18H04498 (H.I.), JP18H01166 (H.O.), and JP19H05631 (H.I., S.T., and M.Y.), by the CASIO Science Promotion Foundation (H.I.), by the Ogasawara Foundation for the Promotion of Science and Engineering (H.I.), by the Program for Interdisciplinary Research in Tohoku University Frontier Research Institute for Interdisciplinary Sciences (H.I.), and CREST, JST Grant Numbers JPMJCR1661 (H.O.) This work was performed under the approval of the Photon Factory Program Advisory Committee (Proposal No. 2016P007, beamline NW10A). M.Y. thanks the support by the 111 project (B18030) from China.

Notes and references

- 1 T. W. Lyons and M. S. Sanford, *Chem. Rev.*, 2010, **110**, 1147–1169.
- 2 (a) D. C. Powers and T. Ritter, *Nat. Chem.*, 2009, **1**, 302–309; (b) M. G. Campbell and T. Ritter, *Chem. Rev.*, 2015, **115**, 612–633.
- 3 J. R. Khusnutdinova, N. P. Rath and L. M. Mirica, *J. Am. Chem. Soc.*, 2010, **132**, 7303–7305.
- 4 L. M. Mirica and J. R. Khusnutdinova, *Coord. Chem. Rev.*, 2013, **257**, 299–314.
- 5 (a) M. G. Campbell, D. C. Powers, J. Raynaud, M. J. Graham, P. Xie, E. Lee and T. Ritter, *Nat. Chem.* 2011, **3**, 949–953; (b) M. G. Campbell, S.-L. Zheng and T. Ritter, *Inorg. Chem.* 2013, **52**, 13295–13297.
- 6 H. Kishida, H. Matsuzaki, H. Okamoto, T. Manabe, M. Yamashita, Y. Taguchi and Y. Tokura, *Nature*, 2000, **405**, 929–932.
- 7 (a) A. L. Beauchamp, D. Layek and T. Theophanides, *Acta Crystallogr., Sect. B: Struct. Crystallogr. Cryst. Chem.*, 1982, **38**, 1158–1164; (b) Y. Wada, T. Mitani, M. Yamashita and T. Koda, *J. Phys. Soc. Jpn.*, 1985, **54**, 3143–3153; (c) S. Kumagai, S. Takaishi, M. Gao, H. Iguchi, B. K. Breedlove and M. Yamashita, *Inorg. Chem.*, 2018, **57**, 3775–3781.
- 8 M. Yamashita and S. Takaishi, *Chem. Commun.*, 2010, **46**, 4438–4448.
- 9 S. Takaishi, M. Takamura, T. Kajiwara, H. Miyasaka, M. Yamashita, M. Iwata, H. Matsuzaki, H. Okamoto, H. Tanaka, S. Kuroda, H. Nishikawa, H. Oshio, K. Kato and M. Takata, *J. Am. Chem. Soc.*, 2008, **130**, 12080–12084.
- 10 S. Kumagai, S. Takaishi, B. K. Breedlove, H. Okamoto, H. Tanaka, S. Kuroda and M. Yamashita, *Chem. Commun.*, 2014, **50**, 8382–8384.
- 11 T. Yoshida, S. Takaishi, H. Iguchi, H. Okamoto, H. Tanaka, S. Kuroda, Y. Hosomi, S. Yoshida, H. Shigekawa, T. Kojima, H. Ohtsu, M. Kawano, B. K. Breedlove, L. Guérin, M. Yamashita, *ChemistrySelect*, 2016, **1**, 259–263.
- 12 M. R. Mian, H. Iguchi, S. Takaishi, H. Murasugi, T. Miyamoto, H. Okamoto, H. Tanaka, S. Kuroda, B. K. Breedlove and M. Yamashita, *J. Am. Chem. Soc.*, 2017, **139**, 6562–6565.
- 13 (a) M. Mitsumi, K. Kitamura, A. Morinaga, Y. Ozawa, M. Kobayashi, K. Toriumi, Y. Iso, H. Kitagawa and T. Mitani, *Angew. Chem., Int. Ed.*, 2002, **41**, 2767–2771; (b) H. Iguchi, S. Takaishi and M. Yamashita, *Chem. Lett.*, 2014, **43**, 69–79; (c) M. Tadokoro, S. Yasuzuka, M. Nakamura, M. Mitsumi, Y. Ozawa, K. Toriumi, H. Yoshino, D. Shiomi, K. Sato, T. Takui, T. Mori and K. Murata, *Angew. Chem., Int. Ed.*, 2006, **45**, 5144–5147; (d) C. H. Hendon, A. Walsh, N. Akiyama, Y. Konno, T. Kajiwara, T. Ito, H. Kitagawa and K. Sakai, *Nat. Commun.*, 2016, **7**, 11950.
- 14 M. R. Mian, H. Iguchi, S. Takaishi, U. Afrin, T. Miyamoto, H. Okamoto and M. Yamashita, *Inorg. Chem.* 2019, **58**, 114–120.
- 15 G. R. Desiraju and T. Steiner, *The Weak Hydrogen Bond*, Oxford University Press, New York, 1999.
- 16 M. R. Mian, H. Iguchi, M. Miyata, S. Takaishi, H. Yamakawa, T. Terashige, T. Miyamoto, H. Okamoto and M. Yamashita, *Z. Anorg. Allg. Chem.*, 2018, **644**, 646–651.
- 17 U. Afrin, H. Iguchi, M. R. Mian, S. Takaishi, H. Yamakawa, T. Terashige, T. Miyamoto, H. Okamoto and M. Yamashita, *Dalton Trans.*, 2019, **48**, 7828–7834.
- 18 (a) R. J. H. Clark, M. Kurmoo, H. J. Keller, B. Keppler and U. Traeger, *J. Chem. Soc., Dalton Trans.*, 1980, 2498–2502; (b) R. J. H. Clark, M. Kurmoo, D. N. Mountney and H. Toftlund, *J. Chem. Soc., Dalton Trans.*, 1982, 1851–1860; (c) H. Tanino and K. Kobayashi, *J. Phys. Soc. Jpn.*, 1983, **52**, 1446–1456.
- 19 R. J. H. Clark, in *Advances in Infrared and Raman Spectroscopy Volume 11*, ed. R. J. H. Clark and R. E. Hester, Wiley, Hayden, 1984, p. 95.

- 20 T. Yoshida, S. Takaishi, S. Kumagai, H. Iguchi, M. R. Mian and M. Yamashita, *Dalton Trans.*, 2019, **48**, 11628–11631.
- 21 (a) N. Kimizuka, *Adv. Polym. Sci.*, 2008, **219**, 1–26; (b) K. Otsubo, Y. Wakabayashi, J. Ohara, S. Yamamoto, H. Matsuzaki, H. Okamoto and H. Kitagawa, *Nat. Mater.*, 2011, **10**, 291–295; (c) K. Otsubo and H. Kitagawa, *CrystEngComm*, 2014, **16**, 6277–6286; (d) K. Otake, K. Otsubo, K. Sugimoto, A. Fujiwara and H. Kitagawa, *Angew. Chem., Int. Ed.*, 2016, **55**, 6448–6451; (e) K. Otake, K. Otsubo, T. Komatsu, S. Dekura, J. Taylor, R. Ikeda, K. Sugimoto, A. Fujiwara, C. Chou, A. W. Sakti, Y. Nishimura, H. Nakai and H. Kitagawa, *Nat. Commun.*, 2020, **11**, 843.
- 22 (a) E. A. Mash, K. A. Nelson, S. Van Deusen, S. B. Hemperly, P. D. Theisen and C. H. Heathcock, *Org. Synth.*, 1990, **68**, 92. (b) A. Scheurer, P. Mosset and R. W. Saalfrank, *Tetrahedron: Asymmetry*, 1997, **8**, 1243–1251.
- 23 M.C. Burla, R. Caliandro, B. Carrozzini, G. L. Cascarano, C. Cuocci, C. Giacovazzo, M. Mallamo, A. Mazzone and G. Polidori, *J. Appl. Cryst.*, 2015, **48**, 306–309.
- 24 G. M. Sheldrick, *Acta Crystallogr.*, 2008, **A64**, 112–122.
- 25 G. M. Sheldrick, *Acta Crystallogr.*, 2015, **C71**, 3–8.
- 26 K. Wakita, Yadokari-XG, Software for Crystal Structure Analyses, 2001; Release of Software (Yadokari-XG 2009) for Crystal Structure Analyses, C. Kabuto, S. Akine, T. Nemoto, E. Kwon, *J. Crystallogr. Soc. Jpn.*, 2009, **51**, 218–224.
- 27 B. Ravel and M. Newville, *J. Synchrotron Radiat.*, 2005, **12**, 537–541.



78x38mm (300 x 300 DPI)